Journal of Inorganic and Organometallic Polymers and Materials (2019) 29:1927–1940
https://doi.org/10.1007/s10904-019-01153-9

Evaluation of the Catalytic Activities of Some Synthesized Divalent and Trivalent Metal Complexes and Their Inhibition Efficiencies for the Corrosion of Mild Steel in Sulfuric Acid Medium

Khadiga M. Takroni[1] · Hoda A. El-Ghamry[1,2] · Ahmed Fawzy[1,3]

Received: 26 February 2019 / Accepted: 8 April 2019 / Published online: 16 April 2019

Abstract
The divalent copper, cobalt, nickel and cadmium in addition to the trivalent iron complexes of the ligand named (E)-1-((4,6-dimethylpyrimidin-2-ylimino)methyl)naphthalen-2-ol were synthesized by the reaction of the ligand with different metal chlorides. The Structures and geometry of the metal chelates have been successfully deduced applying various analytical and spectroscopic tools such as elemental analysis, molar conductance, TGA, magnetic moment measurements, IR, ^{1}H-NMR, EI-mass and UV–Vis spectral studies. The X-ray single crystal structure of the ligand has been also discussed. Spectral studies and analytical results supported the monobasic bidentate behavior of the ligand connecting the metal ion centers via deprotonated phenolic OH and imine nitrogen. In the case of Cu(II) complex, the pyrimidine nitrogen took part in coordination to the Cu center. The results ensured the monometallic character of the chelates having 1:2 (M:L) ratio for copper, cobalt and nickel and 1:1 (M:L) ration for iron and cadmium complexes. The molar conductance data ensured that all the metal complexes are non-electrolytic type of complexes. All the complexes have been proved to have octahedral geometry. The antimicrobial activities of the synthesized metal chelates were evaluated against different bacterial and fungal strains. The synthesized ligand and its complexes were also examined as inhibitors for the corrosion of mild steel in 1.0 M H_2SO_4 at 25 °C using various techniques. The experimental outcomes indicated that the inhibition efficiencies of the tested compounds increased as their concentrations increase. The obtained inhibition efficiencies were interpreted on the basis of strong adsorption of the inhibitor molecules on the surface of mild steel and composing good protection films. The adsorption was found to obey Langmuir adsorption isotherm. The results achieved from all applied techniques are obviously compatible.

Keywords Schiff base · Metal chelates · Structural identification · Corrosion · Inhibitors

1 Introduction

The extensive usefulness of pyrimidine-based compounds is fundamentally due to their implementations in alternative fields such as pharmaceutical, agrochemical, and phytosanitary industries [1, 2]. Recently, there is a great interest in the synthesis of pyrimidine metal complexes due to biological activity including antiviral, antimalarial, antibacterial and antitumor activities [3]. Moreover, numerous number of therapeutics dependent on luminescent heterocyclic metal chelates with interesting characteristics has illustrated in literature, and related complexes may be used in the area of materials science as optical material preparations [4]. Eventually, such compounds may be also employed as significant design for bioinorganic systems, such as metalloproteins, photosensitizers and catalysts [5]. Schiff base metal complexes, as a class of inorganic compounds, are classified as a

Electronic supplementary material The online version of this article (https://doi.org/10.1007/s10904-019-01153-9) contains supplementary material, which is available to authorized users.

✉ Hoda A. El-Ghamry
helghamrymo@yahoo.com

[1] Chemistry Department, Faculty of Applied Science, Umm Al-Qura University, Mecca, Saudi Arabia

[2] Chemistry Department, Faculty of Science, Tanta University, Tanta, Egypt

[3] Chemistry Department, Faculty of Science, Assiut University, Assiut, Egypt

group of compounds of great interest and studied extensively due to their attractive chemical and physical characteristics and their broad range of implementations in different scientific fields. The applications of this class of compounds have been extremely developed in recent years, and such studies have been the subject of many papers and reviews [5–11]. These complexes have wide applications in some biological respects [12–14], organic catalysis [15–17], oxygen carrying [18] and as corrosion inhibitors particularly in acidic medium for alternative alloys and metals [19–22].

Corrosion of metals and alloys is a serious problem and it is receiving more attention by corrosion scientists all over the world because of its dual impacts on both economy and safety. The use of corrosion inhibitors is regarded as one of the most efficient and economical processes to safeguard the surfaces of metals and alloys against corrosion in attacker media. Corrosion inhibitors are usually organic compounds containing hetero atoms, unsaturated bonds and plane conjugated systems [23–27]. Corrosion inhibition by organic compounds is due to their adsorption on the metal surface to form protective layers acting as insulator between the metal surface and the corrosive medium [28–30]. Such adsorption depends on the nature of the metal, the kind and concentration of the corrosive medium and also on the chemical structure of the inhibitor molecule [29]. Furthermore, adsorption of organic inhibitor on the metal surface depends on its functional group, the probable steric effects and electronic density of donor atoms in the inhibitor [31, 32]. On the other hand, steel alloys are major building materials and are widely used in broad areas of industrial applications, and almost in everyday life because of their good mechanical properties. However, these steel alloys and other metals and alloys suffer from corrosion phenomena in some environments [33–35]. Fortunately, the synthesized ligand (HL) and its complexes (**C1** to **C5**) are compounds that involve hetero atoms such as N and O, unsaturated bonds and plane conjugated systems in their structures which make them worthy to be employed in the area of corrosion inhibition of metals and alloys [30–33]. Based on these facts, the objectives of the current study are extended to investigate (HL) and its complexes (**C1** to **C5**) as corrosion inhibitors for mild steel in sulfuric acid solutions using alternative techniques and compare between them in their inhibition efficiencies.

2 Experimental

2.1 Materials and Methods

2-Amino-4,6-dimethylpyrimidin, 2-hydroxy-1-naphthaldehyde and all other chemicals and solvents used in the current study were purchased from Aldrich, Merck and/or across companies and have been used as received. CHN content of the new synthesized compounds were analyzed using Perkin-Elmer 2400 CHN Elemental instrument. Infrared spectra were recorded by the aid of Perkin–Elmer 1430 IR spectrophotometer at 4000–400 cm^{-1} range as KBr disks. EI-MS of the ligand was recorded at 70 eV. The ^{1}H-NMR spectra were carried out using a Varian Mercury Oxford NMR 300 Hz spectrophotometer after dissolving the samples in DMSO d^6 using tetramethylsilane as internal standard by dissolution of the ligand in d^6-DMSO. Molar conductance of metal chelates dissolved in DMF was measured from 10^{-3} M solutions at 25 °C using a 523 conductivity bridge instrument. The thermogravimetric analysis (TGA) of the synthesized compound was measured by the aid of Schimadzu TG-50 thermogravimetric instrument at 10 °C/min heating rate under N_2 environment from ambient temperature up to 800 °C. The UV–Vis spectra were measured on a Shimadzu UV–Vis 240 spectrophotometer. The magnetic susceptibilities of the solid chelates were measured at 25 °C using Gouy's method. Thermostated PGSTAT30 potentiostat/galvanostat connected to a three-electrode electrochemical cell was used to evaluate the inhibition efficiencies of the synthesized compounds using potentiodynamic polarization (PP) and electrochemical impedance spectroscopy (EIS) techniques. The working electrode was a mild steel rod pressing into a Teflon holder in which the electrode area which is in direct exposure to the corrosive media was 0.5 cm^2. Before each experiment the working electrode was contemporized as previously reported [23, 24], then it was placed immediately into 1.0 M H_2SO_4 (corrosive medium, blank) and/or the desired inhibitor concentration at open circuit potential (OCP) until a steady state was reached.

2.2 Synthesis of the Schiff Base HL

Schiff base compound named (E)-1-(((1H-benzo[d]imidazol-2-yl)methylimino) methyl)naphthalen-2-ol was obtained by modification of the previously reported method [36] in which 1.72 g (0.01 mol) of 2-hydroxy-1-naphthaldehyde dissolved in 30 ml of boiled EtOH was slowly added to a 30 ml of boiled and stirred ethanolic solution containing 2-amino-4,6-dimethyl pyrimidine (1.23 g, 0.01 mol). The obtained mixture was then allowed to reflux for half an hour through which bright yellow poly crystalline precipitate was obtained. The resulting precipitate was directly filtered off, rinsed three times with EtOH followed by ether and eventually dried under vacuum. Needles like crystals of the ligand suitable for X-ray single crystal measurements were obtained by slow vaporization of ethanolic solution of the ligand over 3 days. Yield: 2.38 g (85%).m.p. 186 °C. Anal. Calcd (%) for HL($C_{17}H_{15}N_3O$; 277.32 g mol^{-1}): C, 73.63; H, 5.45; N, 15.25. Found: C, 73.49; H, 5.46; N, 15.37. EI-mass spectra m/z = 277. IR (cm^{-1}, KBr phase): 3422(w, br), 1627(s), 1538(s), 1202(m). ^{1}H NMR (300 MHz, DMSO-d^6, δ, ppm):

δ: 14.35 (s, 1H, ArOH), 9.506 (s,1H, CH=N), 8.148–6.637 (d or m, 6H, Ar–H), 6.214 (s, 1H, $CH_{pyrimidine}$), 2.157 (s, 6H, CH_3).

2.3 Synthesis of Metal Chelates (C1–C5)

The metal chelates (**C1**–**C5**) are synthesized by slow addition of a hot methanolic solution containing 0.001 mol of the metal chlorides (0.17 g of $CuCl_2{\cdot}2H_2O$, 0.238 g of $CoCl_2{\cdot}6H_2O$, 0.237 g of $NiCl_2{\cdot}6H_2O$, 0.27 g of $FeCl_3{\cdot}6H_2O$ or 0.183 g of $CdCl_2$) to a hot methanolic solution containing 0.277 g (0.001 mol and 20 ml) of HL. The resulting mixtures were allowed to heat under reflux for 4 h at 70 °C within which colored products were formed. The products were separated from the hot solutions by vacuum filtration, washed with methanol and ether and finally dried under vacuum.

2.4 Determination of Single Crystal Structure

Structure determination of **1** was done at the National research center in Egypt through a Kappa CCd Enraf–Nonius FR 90 four circle goniometer having graphite monochromatic MoKα radiation {[λMoKα] = 0.71073 Å} at 25 ± 2 °C. Direct methods were used in solving the structure of HL [37]. All of the non H-atoms were placed from the primary solution or from subsequent electron density difference maps through the primary refinement procedures. After all the non H-atoms in the compound construction are located, the model was refined against F2, at first by the use of isotropic displacement parameters and finally by using anisotropic ones. Positions of H-atoms were calculated and refined isotropically, and the final cycle of refinements was achieved.

2.5 Antimicrobial Activity

Antimicrobial efficiency of the compounds under interest was tested using disc-agar diffusion method [38] against the sensitive microorganisms *Escherichia coli* as Gram-negative bacteria, *Staphylococcus aureus* as Gram-positive bacteria, *Aspergillus flavus* and *Candida albicans* as fungi. Standard discs of Tetracycline (Antibacterial agent), Amphotericin B (Antifungal agent) used as +ve controls for antimicrobial efficiency. Filter discs immersed in 10 µl of dimethyl sulfoxide were used as a −ve control [12].

2.6 Corrosion Inhibition Experiments

Corrosion and corrosion inhibition tests were carried out on mild steel rods of the composition (wt%): 0.07% C, 0.07% Si, 0.012% S, 0.021% P, 0.29% Mn and the remainder is iron. Weight-loss (WL) experiments were performed on cylindrical rods of mild steel with areas closed to 10 cm^2 and were prepared for these measurements as mentioned earlier [23, 24]. The corrosion rate (CR) was determined in mpy using the following equation [39]:

$$\mathrm{CR} = \frac{KW}{Atd} \tag{1}$$

where K is a constant (3.45×10^6), W is the weight loss in mild steel sample in grams, A is the exposed sample area in cm^2, t is time in hours and d is the density of steel sample in g/cm^3. The inhibition efficiency (% IE) of the inhibitors was calculated by the following equation [39]:

$$\%\ \mathrm{IE} = \theta \times 100 = \left[1 - \frac{CR_{inh}}{CR}\right] \times 100 \tag{2}$$

where CR and CR_{inh} are the values of corrosion rate in the absence and presence of inhibitor, successively.

In both PP and EIS technique the values of % IE of the inhibitors were calculated as reported earlier [23, 24].

3 Results and Discussion

The synthesized chelates were found to be highly stable in air. They are slightly soluble in methanol and ethanol while easily soluble in DMSO and DMF and completely insoluble in water, hexane and diethyl ether. Molar conductivity values of 10^{-3} M solution of compounds **C1**–**C5** in DMF are within 12.5–19.6 $O^{-1}cm^2\ mol^{-1}$ range, confirming the non-electrolytic manner of such chelates. On the basis of elemental analysis and mass spectral results, the complexes were assigned the composition shown in Table 1.

3.1 Crystal Structure of the Ligand HL

Crystal structure of the organic ligand HL was identified using X-ray single crystal measurement. The crystallographic data in addition to the refinement parameters are depicted in Table S1; bond lengths and angles are presented in Tables S2 and S3. Crystallographic data showed that HL crystallizes in monoclinic with P21/n space group. The asymmetric unit contains one ligand molecule; Fig. 1. The naphthyl and pyrimidine moiety attached to the azomethine group are oriented in a trans fashion as expected. All the bond lengths are found to be within the normal values when compared with correlated ligands [40, 41]. The molecule is found to exhibit good planarity. The plane compressing the naphthyl carbon is canted with respect to the plane containing the 4,6-dimethylpyrimidine ring atoms at angle of 2.84°.

The conformation of the molecule is stabilized by one intramolecular hydrogen bond that is O1–H1···N4 and no intermolecular hydrogen bonds are involved (Fig. 2). The

Table 1 Elemental analysis data and some physical properties of the organic ligand and its metal complexes

Compound No.	Structure	Color (Λ_m)[a]	m.p (yield %)	Elemental analysis cal. (found) C%	H%	N%	M%[c]	Mol. wt.
HL	$C_{17}H_{15}N_3O$	Yellow	186 84	73.63 (73.49)	5.45 (5.46)	15.25 (15.37)	–	277.32
C1	$[L_2Cu]$ $C_{34}H_{28}CuN_6O_2$	Brown (12.5)	256[b] 56	66.27 (66.36)	4.58 (4.66)	13.64 (13.73)	10.31 (10.62)	616.17
C2	$[L_2Co(H_2O)_2]H_2O$ $C_{34}H_{34}CoN_6O_5$	Deep yellow (15.3)	260[b] 67	61.35 (61.53)	5.15 (5.24)	12.63 (12.41)	8.85 (8.15)	665.6
C3	$[L_2Ni(H_2O)_2]2H_2O$ $C_{34}H_{36}NiN_6O_6$	Yellowish green (18.5)	> 300	59.76 (59.57)	5.31 (5.12)	12.30 (12.18)	8.59 (8.12)	683.38
C4	$[LFe(H_2O)_2Cl_2]0.5H_2O$ $C_{17}H_{19}Cl_2FeN_3O_{3.5}$	Dark Brown (15.7)	142	45.57 (46.81)	4.27 (4.72)	9.38 (9.25)	12.46 (12.17)	448.1
C5	$[LCd(H_2O)_3Cl]$ $C_{17}H_{20}CdN_3O_4$	Brown (19.6)	290[b]	42.70 (42.65)	4.22 (4.12)	8.79 (8.63)	23.51 (23.02)	478.22

[a]Calculated from mass spectrum

[b]Decomposition temperature

[c]Calculated from thermal analysis

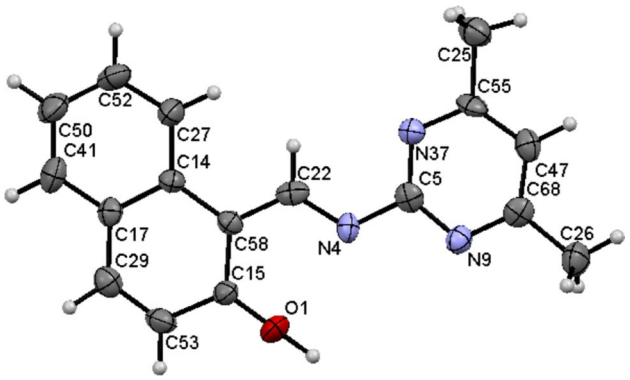

Fig. 1 Molecular structure of HL showing the atom-labeling scheme. Displacement ellipsoids are drawn at the 50% probability level

compound displayed no obvious face-to-face π stacking interaction between the adjacent aromatic rings (Fig. 2).

3.2 NMR Spectra

^{1}H-NMR spectra of the ligand (HL) and Cd(II) complex **C5** were recorded in d^6-DMSO using tetramethylsilane (TMS) as internal standard (Figs. 3, 4). The ligand spectrum displayed two resonances at 14.35 and 9.5 ppm that to the phenolic OH and CH=N protons, respectively [37]. The signal appearing at 14.35 ppm completely disappeared upon adding D_2O confirming its assignment to OH group. Pyrimidine CH proton appeared as singlet at 7.05 ppm [36]. The aromatic protons of the naphthyl ring featured as doublet and multiplet signals in the range 8.9–6.21 ppm and the six protons of the methyl groups appeared as singlet at 2.15 ppm [36, 42].

In the spectra of Cd(II) complex **C5**, electron density shift from the ligand to the metal is observed which strongly supported the deprotonation of the phenolic group [43]. Signal of azomethine proton appeared deshielded at 10.77 ppm, compared to 9.5 ppm in the HL, supporting its coordination to the metal center via nitrogen atom [43, 44]. The aromatic protons of the naphthyl ring appeared almost at the same positions as in the ligand, with small shift in some signals as doublet and multiplet signals within the range 8.82–6.43 ppm while methyl groups protons appeared overlapped with the solvent protons.

3.3 Mass Spectroscopy

Mass spectra of the ligand and its complexes have been measured in order emphasize the composition and pureness of the isolated complexes. Figure 5 shows the EI-mass spectrum of complex **C4**, as an example, and its fragmentation pathways are indicated in Scheme 1. The mass spectrum of HL and complexes **C1**–**C3** and **C5** are illustrated in Figs S1–S5 Mass spectra of HL and complexes **C1** and **C5** showed the molecular ion peak at m/z 277, 616 and 478, respectively. These fragments assigned to the predicted molecular weights of the compounds. For complex **C2** and **C4** the molecular ion peak appeared at m/z 663 and 451 that assigned to M^{-2} and M^{+3}, respectively. For compound **C3**, the molecular ion peak assigned to the molecular weight of the compound without H_2O of crystallization. Spectrum of complex **C4** showed fragments at m/z 451, 437, 420, 403, 331 and 305 which assigned to the fragments having the formulae $[LFe(H_2O)_2Cl_2]0.5H_2O$, $[LFe(H_2O)_2Cl_2]$, $[LFe(H_2O)Cl_2]$, $[LFeCl_2]$, [LFe] and [L′Fe] (where L′ is 1-(Pyrimidin-2-yliminomethyl)-naphthalen-2-ol); calcd. molecular weights are 448, 439, 421, 403, 332 and 304, respectively, confirming the formation of the complex as proposed.

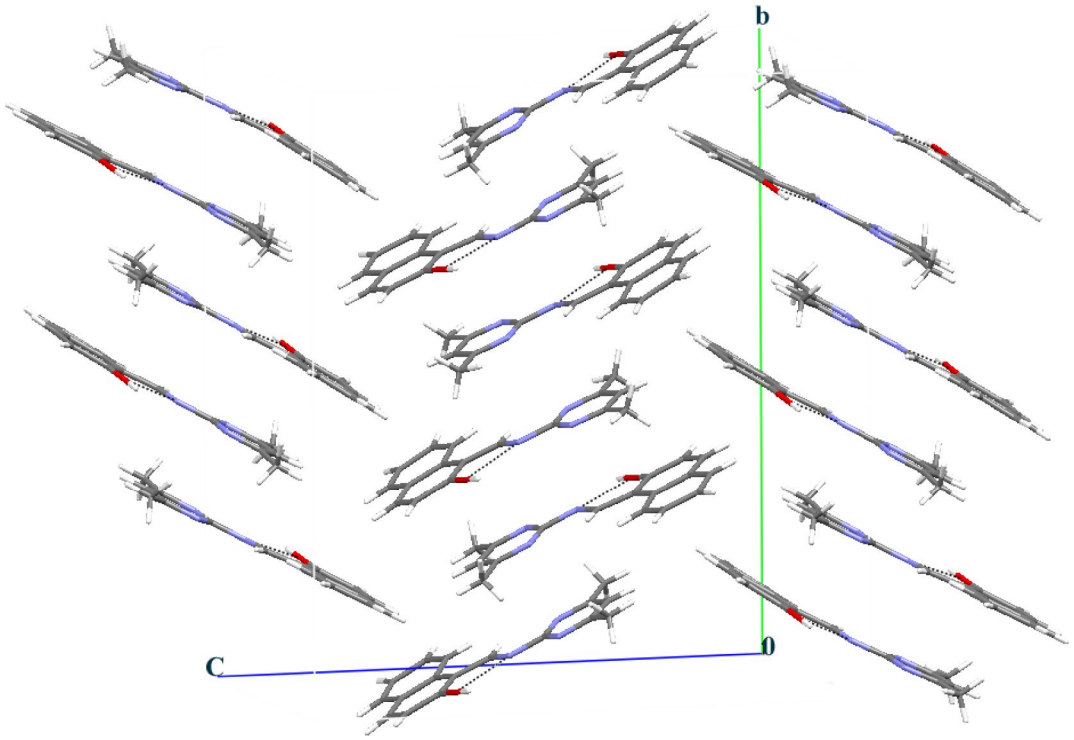

Fig. 2 Two-dimensional view of HL along bc plane indicating the one intramolecular hydrogen bonds O–H···N

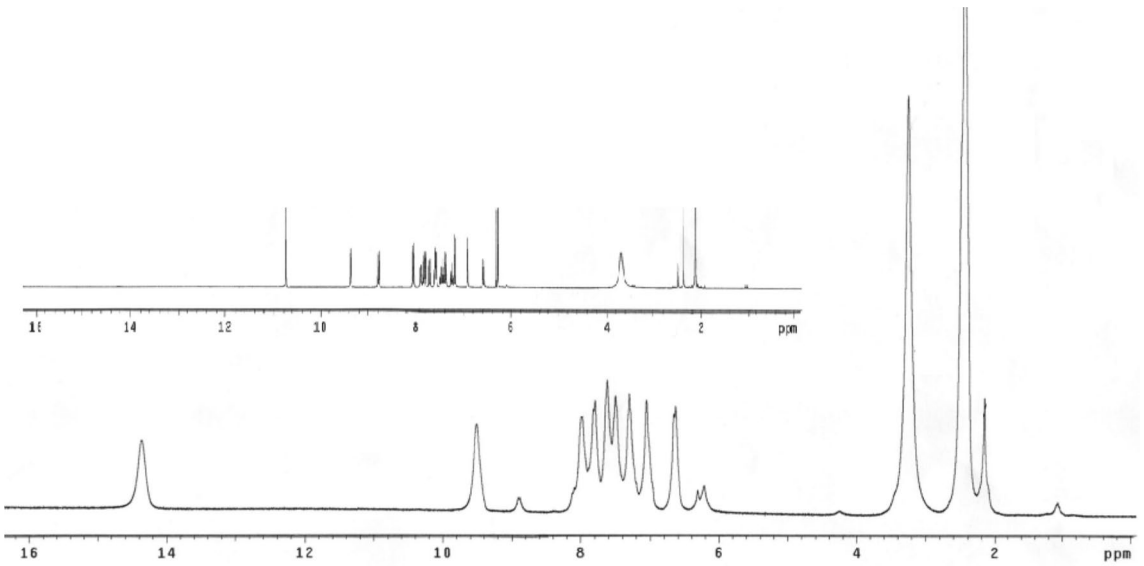

Fig. 3 ^{1}H-NMR spectrum of HL in d^{6}-DMSO (*inset* ^{1}H-NMR spectrum of HL in D_2O)

3.4 FTIR Spectral Studies

Explanation of the IR spectra is a very beneficial method that is used to assure the mode of binding of ligand to metal ion. IR spectra of the ligand and complexes C1–C5 are illustrated in Fig. S6 while the most significant IR spectral bands that are used to identify the ligand function groups which bind to the metal ion are depicted in Table 2. The spectrum of HL exhibited two peaks at 1627 and 1538 cm^{-1} assigned to υ(C=N) of the imine group and pyrimidine ring, respectively. The first band (of imine

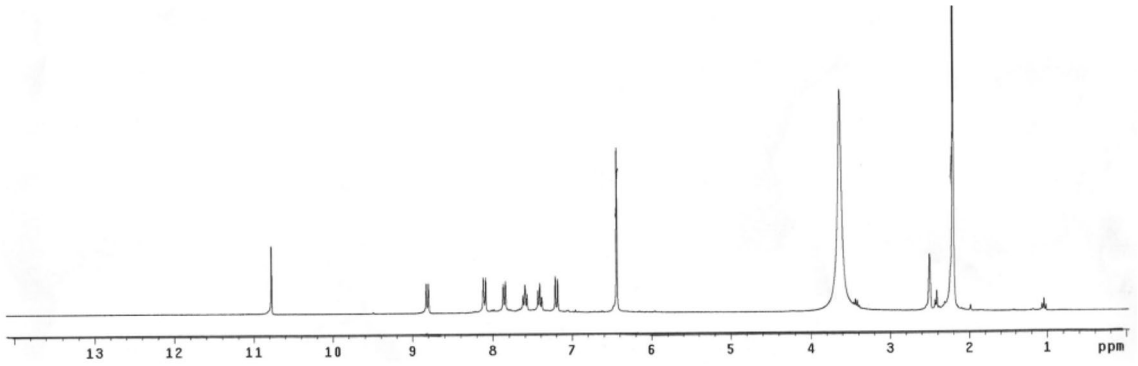

Fig. 4 ^{1}H-NMR spectrum Cd(II) complex **C5** in d^{6}-DMSO

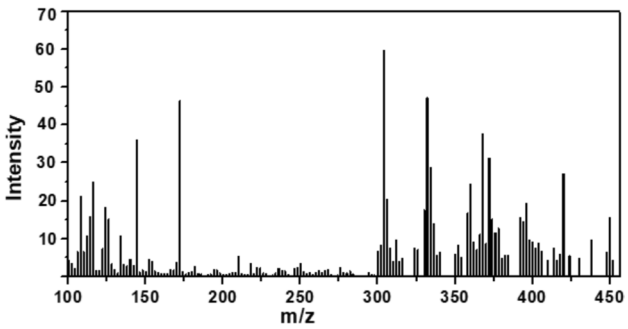

Fig. 5 Mass spectrum of complex **C4**

group) underwent a shift in its place to higher or lower wavenumbers by 13–21 cm^{-1} in complexes spectra which supports the involvement of azomethine nitrogen atoms in bond formation with the metal ion center [37]. On the other hand, the second band corresponding to υ(C=N) of pyrimidine ring appeared nearly at the same place in the spectra of metal chelates indicating that this band is not taking part in coordination to the metal center except for complex **C1** in which the shift of such by 13 cm^{-1} is an evidence for its participation in complex formation through M–N bond formation. The evidence of the participation of the phenolic-O in coordination to the metal ion could not be obtained unambiguously by the broad and strong band appeared around 3400 cm^{-1} as a result of the presence of crystallization H_2O molecules however the downfield shift in the ligand band appearing at 1202 cm^{-1}, which assigned to υ(C–O), by 7–20 cm^{-1} in the spectra of metal chelates strongly supported the involvement of the phenolic-O in coordination to the metal center after deprotonation [45].The non-ligand bands which appeared in the spectra of metal chelates in 510–550 and 454–480 cm^{-1} ranges corresponding to υ(M–O) and υ(M–N) and confirm the involvement of the azomethine nitrogen and phenolic oxygen to the metal center [37].

3.5 Thermogravimetric Analysis

The thermal character and thermal stability of metal chelates was studied and clarified by interpretation of their TG curves. Interpretation of the thermoanalytical data of the metal chelates C1–C5 are detailed in Table 3 and their thermograms are shown in Figs. S7–S11.

Analysis of the metal complexes thermograms showed that complexes C1, C2 and C3 underwent degradation within three sequential stages, complex C5 decomposed within four stages whereas complexes C4 decomposed through five steps through the temperature range 28–800 °C. For complexes C2, C3 and C5, the first degradation step appeared in the ranges 28–165, 28–159 and 96–186 °C, respectively, and specified to the evaporation of lattice and/or coordinated water molecules; for compound C1, the first step appeared at 193–232 °C and assigned to the loss of four methyl attachments and azomethine moiety. The second decomposition step appeared within the ranges 231–528, 165–338, 159–371 and 186–256 °C for complexes C1, C2, C3 and C5, respectively, which analyzed to be corresponding to the loss of two pyrimidine moieties from compound C1, one naphthalene ring and two methyl attachments for compound C2 and two methyl groups + one coordinated chloride ion in addition to azomethine moiety for compound C5. The organic ligand decomposed through the last step of decomposition appearing within the ranges 528–790, 338–776, 371–686, 256–705 °C for C1, C2, C3 and C5, respectively, leading to the fashioning MO as thermally stable product. Fe(III) complex C4 decomposed in five sequent degradation stages. The first and second step of decomposition appeared at 28–89 and 89–197 °C and specified to the vaporization of half molecule of lattice water and two methyl groups, respectively. Both coordinated water and chloride ions are lost within the third stage of decomposition appearing at 197–426 °C. The organic

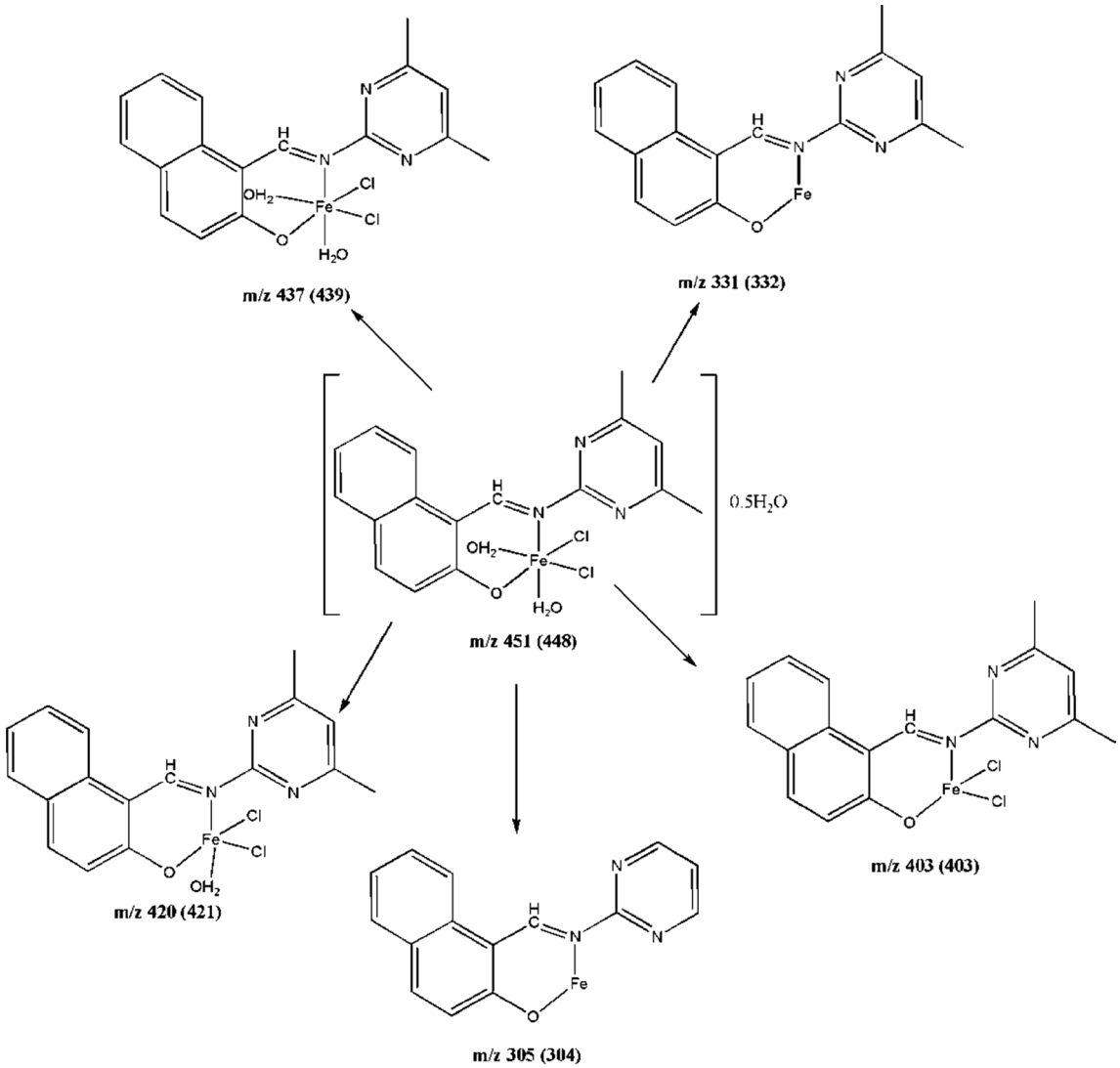

Scheme 1 Fragmentations pathways of **C4**

Table 2 IR spectral data of organic ligand and its metal complexes

Compound	ν_{OH}	$\nu_{C=N}$ *ring*	$\nu_{C=N}$ *imine*	ν_{C-O}	ν_{M-O}	ν_{M-N}
HL	3422	1627	1538	1202	–	–
C1	–	1610	1525	1182	550	454
C2	3389	1640	1539	1185	516	457
C3	3414	1641	1539	1187	521	457
C4	3410	1606	1535	1195	510	458
C5	3422	1643	1537	1182	524	480

Table 3 The decomposition steps, temperature range, calculated and found weight loss of the prepared complexes

Complex no. (M wt)	Temp. range (°C)	Mass loss %		Assignment
		Calc.	Found	
C1	28–193	–	–	Thermal stability
$[L_2Cu]$	193–232	14.11	13.68	Loss of 4 methyl + 1 CH=N moieties
(616.17)	231–528	24.99	24.82	Loss of 2 pyrimidine moieties
	528–790	47.92	48.11	Further decomposition of the ligand with the formation of CuO residue
		10.31	10.62	% of Cu content
C2	28–165	10.53	10.06	Loss of 1 lattice and 2 coordinated H_2O molecules
$[L_2Co(H_2O)_2]H_2O$	165–338	22.84	23.37	Loss of 1 naphthalene ring + 2 methyl groups
$C_{34}H_{34}CoN_6O_5$	338–776	52.13	52.76	Further decomposition of the ligand with the formation of CoO residue
(665.6)		8.62	8.15	% of Co content
C3	28–159	10.53	10.79	Loss of 2 lattice H_2O and 2 coordinated H_2O
$[L_2Ni(H_2O)_2]2H_2O$	159–371	31.35	31.90	Loss of 2 moieties of 4,6-dimethylpyrimidine
(683.38)	371–686	47.17	47.34	Further degradation of the ligand with the formation of NiO residue.
		8.59	8.12	% of Ni content
C4	28–89	2.01	2.59	Loss of 0.5 lattice H_2O molecules
$[LFe(H_2O)_2Cl_2]$ $0.5H_2O$	89–197	6.70	6.26	Loss of 2 methyl groups
(448.1)	197–426	23.70	23.27	Loss of 2 coordinated H_2O + 2 coordinated Cl^-
	426–641	17.22	16.71	Loss of pyrimidine moiety
	641–796	33.00	32.58	Further degradation of the ligand with the formation of $0.5Fe_2O_3$ + C residue
		12.46	12.17	% of Fe content
C5	28–96	–	–	Thermal stability
$[LCd(H_2O)_3Cl]$	96–186	11.29	11.30	Loss of three coordinated H_2O molecules
(478.22)	186–256	19.34	19.67	Loss of 2 methyl + 1coordinated Cl^-+CH=N
	256–318	5.85	5.83	Decomposition of pyrimidine ring with the loss of N_2
	318–705	37.05	42.73	Further degradation of the ligand with the formation of CdO residue
		23.51	23.02	% of Cd content

ligand decomposed within the last two successive steps appearing at 426–641 and 641–796 leading to the formation of Fe_2O_3 as thermally stable oxide along with carbon residue.

3.6 Electronic Spectra and Magnetic Moments

Electronic spectroscopic tool is extremely effective way to distinguish between the different geometrical structures around the metal center. It is also a useful tool to be sure of the binding of ligand to the metal centers. The UV–Vis spectrum of HL and its metal chelates (**C1**–**C5**) were recorded using the Nujol mull method (Fig. S12). The free ligand showed intense bands at 287 and 305 nm assigned to $\pi \rightarrow \pi^*$ and $n \rightarrow \pi^*$ transitions of the azomethine group [46]. In case of complexes spectra, the first band appeared at 294, 297, 275, 297 and 268 nm and the second band appeared at 316, 317, 300, 317 and 309 nm in the spectra of **C1**, **C2**, **C3**, **C4** and **C5**, respectively. The red or blue shift in the place of such bands in the spectra of metal chelates, **C1**–**C5**, supports the coordination of the ligand to metal ion via the azomethine nitrogen [47].

In addition to these bands, UV–Vis spectrum of the Cu(II) complexes **C1** exhibited absorption band at 587 nm that specified to $^2E_g \rightarrow {}^2T_{2g}$ transition reported for octahedral configuration [48, 49]. μ_{eff} value of **C1** has been calculated to be 1.83 B.M corresponding to an unpaired electron in Cu^{2+} center as expected.

The electronic spectra of Co^{2+} complex **C2** exhibited 2 bands at 548 and 630 nm assignable to $^4T_{1g}(F) \rightarrow 4T_{1g}(p)$ and $^4T_{1g}(F) \rightarrow {}^4A_{2g}(F)$ transitions, successively, assignable to octahedral geometrical structure [50]. Co(II) complex **C2** had magnetic moment of 4.43 B.M which is distinctive of high-spin octahedral chelates [51].

The electronic spectrum of Ni^{2+} complex **C3** showed 2 bands in Nujol mull at 427 and 631 nm corresponding to $^3A_{2g} \rightarrow {}^3T_{1g}(P)$ and $^3A_{2g} \rightarrow {}^3T_{1g}(F)$ transitions, respectively, which confirmed octahedral arrangement around the nickel center. μ_{eff} value of this complex was found to be 3.21 B.M supporting the octahedral arrangement in Ni(II) compound [52].

Iron(III) complex **C4** exhibited three spectral bands at 486, 579 and 645 nm which assigned to $^6A_{1g}(S) \rightarrow {}^4A_{1g}(G)$, $^6A_{1g}(S) \rightarrow {}^4T_{2g}(G)$ and $^6A_{1g}(S) \rightarrow {}^4T_{1g}(G)$ transitions

indicative of high-spin octahedral geometry [53]. μ_{eff} value of **C4** was found to be 5.6 B.M. supporting the octahedral high-spin d^5 configuration of octahedral Fe(III) complex.

Cadmium(II) complex with d^{10} configuration can only show the charge transfer (CT) transitions which can be specified to charge transfer from the ligand to the metal and vice versa, no d–d transition are predicted [37, 43]. The electronic spectrum of **C5** displayed two non-ligand bands at 447 and 530 nm specified to CT transition. The apparent shift in ligand bands the proof for complex formation [54]. Also as predicted, their electronic spectra did not provide much useful knowledge about stereochemistry. Complex **C5** is diamagnetic, as predicted.

As a conclusion of the previous analytical and spectral results, the structures of the metal chelates **C1**–**C5** can be represented as shown in Scheme 2.

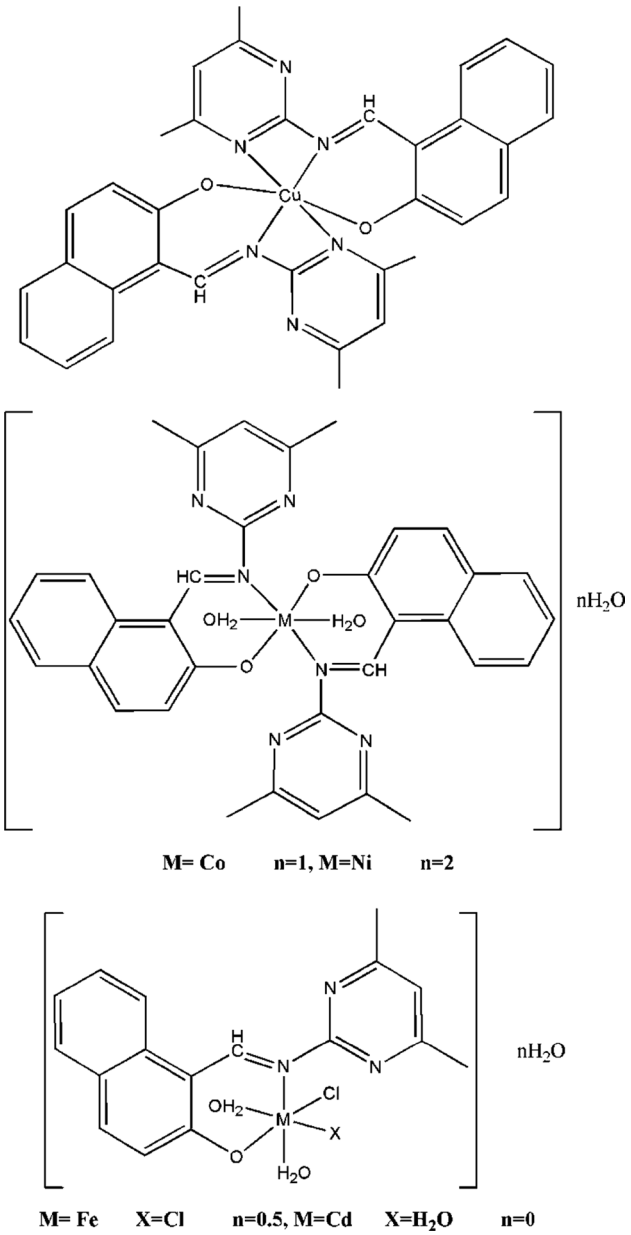

Scheme 2 Structures of the synthesized compounds **C1**–**C5**

3.7 Antimicrobial Activity

Schiff base ligand (HL) and its metal complexes were tested in vitro for antibacterial effectiveness against the different pathogenic Gram +ve bacteria *Bacillus subtilis* and *Staphylococcus aureus*, Gram −ve bacteria *Escherichia coli* and *Pseudomonas aeruginosa* and the fungal strains *Aspergillus flavus* and *Candida albicans*. The inhibition zone diameter in (mm/mg sample) were measured and recorded in Table 4. The obtained results represents that the organic ligand HL was completely inactive against all the tested bacterial. On the other hand, the tested metal chelates afforded high efficiency against the tested bacterial and fungal micro-organisms. Most of the metal chelates afforded the highest inhibition zone diameter against the bacterial strains *Pseudomonas aeruginosa* which is nearly equal to that of the slandered drug Ampicillin in the case of **C1** and **C4**. The promising data was shown by the cadmium complex **C5** which showed relatively higher efficiency against all the examined strains when compared with the slandered drugs Ampicillin and Amphotericin B. Compound **C3** showed the least activity against the tested strains when compared with the other complexes and slandered drugs. The activity of the tested metal chelates follow the order **C5** > **C4** > **C2** > **C1** > **C3**. The increased activity of the metal complexes when compared with the inactive ligand can be in general interpreted on the basis overton's concept and Tweedy's chelation theory [55].

3.8 Evaluation of the Inhibition Efficiencies of the Synthesized Compounds

3.8.1 Weight-Loss Measurements

WL measurements of mild steel in 1.0 M H_2SO_4 were performed in the absence and existence of different concentrations of the ligand (HL) and its complexes (**C1**–**C5**) in the concentration range (200–800 ppm) at 25 °C. For briefly, weight-loss versus time curves obtained for the ligand HL is represented in Fig. 6. CR values of mild steel and % IE of all tested compounds are also calculated and listed in Table 5. The results indicated that CR values decreased with the inhibitor concentration which due to increased adsorption coverage of the inhibitor on the surface of mild steel with the inhibitor concentrations resulting in decrease in the dissolution rates of steel alloy by blocking the corrosion sites spread on the iron surface. Thus, the synthesized compounds can be considered as effective inhibitors for mild

Table 4 Inhibition zone diameter (mm/mg sample) of the tested compounds against number of bacterial and fungal strains

Comp.	Inhibition zone diameter (mm/mg sample)					
	Bacterial species				Fungi	
	(G+)		(G−)			
	Bacillus subtilis	*Staphylococcus aureus*	*Escherichia coli*	*Pseudomonas aeruginosa*	*Aspergillus flavus*	*Candida albicans*
Control: DMSO	0.0	0.0	0.0	0.0	0.0	0.0
Ampicillin Antibacterial agent	26	21	25	26	–	–
Amphotericin B Antifungal agent	–	–	–	–	17	20
HL	0.0	0.0	0.0	0.0	0.0	0.0
C1	21	19	22	25	13	11
C2	24	20	23	21	15	12
C3	17	13	16	18	11	11
C4	23	19	24	25	15	14
C5	40	27	37	38	21	23

steel corrosion in the investigated aggressive medium (1.0 M H_2SO_4). Careful inspection of the results (listed in Table 5 and illustrated in Fig. 7) showed that, at the same inhibitor concentration, the inhibition efficiencies follows the order: **HL > C5 > C4 > C1 > C2 > C3** indicating that the possible steric effects and electronic density of donor atoms of the compound are considered as the main roles in the adsorption process.

3.8.2 Potentiodynamic Polarization (PP) Measurements

The PP measurements for mild steel in 1.0 M H_2SO_4 in the absence and existence of various concentrations of the synthesized compounds are carried out (only PP curves obtained for the complex **C2** as a representative example are only shown here in Fig. 8) and the associated corrosion parameters are evaluated and are depicted also in Table 1. The data represented that addition of fixed concentrations of the investigated compounds to the blank solution shifted both anodic and cathodic branches of the polarization curves towards lower current density values which point out the retardation of both anodic and cathodic reactions resulting in an inhibition of iron corrosion. Since, the inhibitor exhibited anodic and cathodic inhibition effects with slightly shift in E_{corr} value to more anodic potentials, it could be deduced that such synthesized compounds perform as mixed-type inhibitors with anodic domination [56]. The values of % IE were found to increase with increasing inhibitors concentrations and the extent of inhibition efficiencies of the compounds, at the same concentration, followed the order: **HL > C5 > C4 > C1 > C2 > C3**, in consistent with the results obtained from WL measurements.

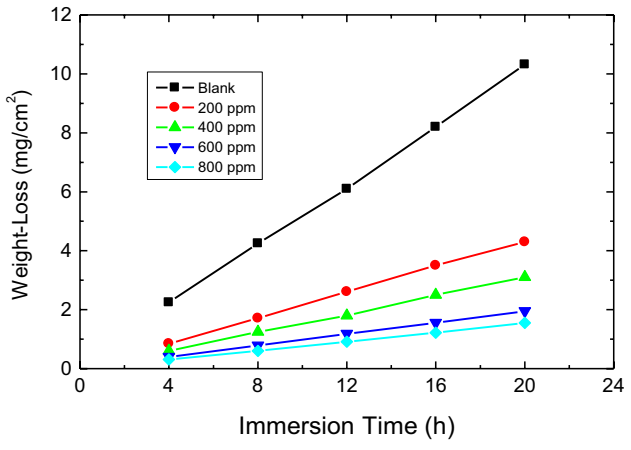

Fig. 6 Weight-loss versus immersion time for mild steel in 1.0 M H_2SO_4 solution in the absence and presence of different concentrations of the ligand HL at 25 °C

3.8.3 Electrochemical Impedance Spectroscopy (EIS) Measurements

Corrosion of mild steel in 1.0 M H_2SO_4 solution was also examined by EIS measurements. Nyquist plots of mild steel corrosion in 1.0 M H_2SO_4 solution containing various concentrations of the synthesized compounds are plotted but only Nyquist plots for the complex C4 is illustrated in Fig. 8. The values of R_{ct} and %IE are also listed in Table 1. Figure 9 illustrated that, for all examined compounds, the size of the capacitive semicircle of mild steel in the corrosive medium (1.0 M H_2SO_4 solution) increased significantly after the addition of the inhibitor indicating a decrease in the rate of mild steel corrosion, and this behavior increased with increasing inhibitor concentration. Also, increasing R_{ct} value with the inhibitor concentration indicates that the

Table 5 Corrosion parameters of mild steel in 1.0 M H_2SO_4 solution and the values of % IE of the synthesized compounds obtained from the three employed techniques (WL, PP and EIS) at 25 °C

Inh.	Concn. (ppm)	WL		PP					EIS	
		CR	% IE	$-E_{corr}$ (mV(SCE)	β_a (mV/dec.)	$-\beta_c$ (mV/dec.)	i_{corr} (μA/cm^2)	% IE	R_{ct}	% IE
	0	225	–	497	52	47	518	–	32	–
HL	200	95	58	493	65	74	191	63	91	65
	400	68	70	478	72	79	129	75	133	76
	600	43	81	475	73	99	83	84	215	85
	800	34	85	469	81	105	57	89	355	91
C1	200	110	51	503	59	68	233	55	78	59
	400	77	66	495	68	75	166	68	106	70
	600	54	76	483	73	84	119	77	145	78
	800	45	80	484	85	97	109	79	168	81
C2	200	117	48	491	61	97	254	51	71	55
	400	92	59	480	74	110	207	60	95	66
	600	61	73	471	81	112	145	72	125	74
	800	52	77	466	102	129	124	76	152	79
C3	200	126	44	493	69	88	249	52	67	52
	400	99	56	491	71	89	192	63	89	64
	600	65	71	485	82	102	150	71	119	73
	800	56	75	479	95	104	119	77	145	78
C4	200	106	53	502	72	89	202	61	76	58
	400	77	66	504	73	95	150	71	107	70
	600	52	77	492	84	105	109	79	160	80
	800	43	81	487	83	99	93	82	188	83
C5	200	101	55	490	69	102	201	61	80	60
	400	72	68	481	81	105	140	73	110	71
	600	51	77	469	82	107	98	81	178	82
	800	38	83	473	79	111	78	85	202	84

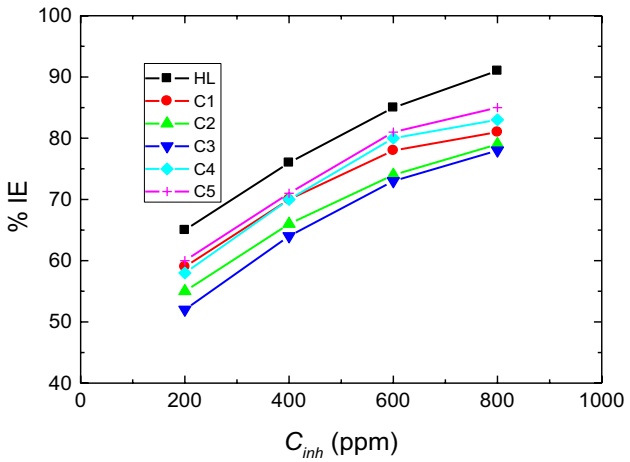

Fig. 7 Comparison between the inhibition efficiencies of the synthesized ligand (HL) and its complexes (**C1** to **C5**) for the corrosion of mild steel surface in 1.0 M H_2SO_4 solution at 25 °C

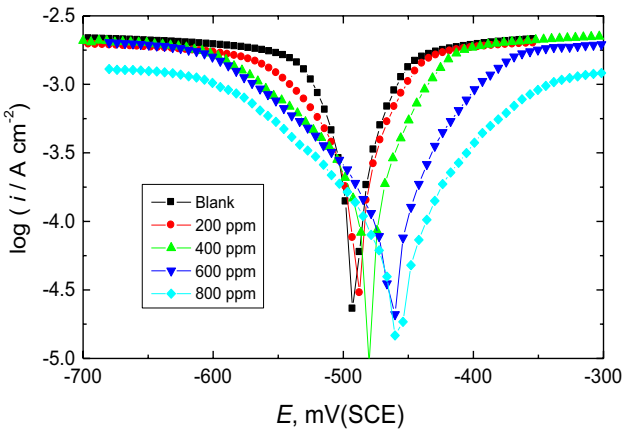

Fig. 8 Potentiodynamic polarization curves for mild steel corrosion in 1.0 M H_2SO_4 solution in the absence and presence of different concentrations of the complex C2 at 25 °C

number of the inhibitor molecules adsorbed on the surface of mild steel increases resulting in increasing the inhibition efficiency [57].

3.8.4 Adsorption Isotherm

Alternative adsorption isotherms like Temkin, Langmuir, Freundlich, Frumkin, Bockris–Swinkels and Flory–Huggins, can

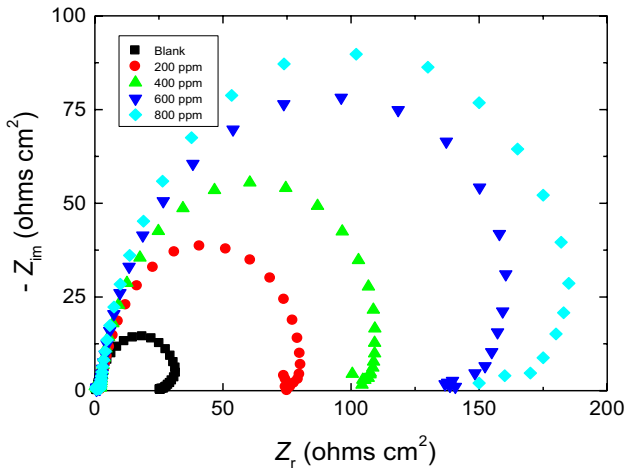

Fig. 9 Nyquist plots for the corrosion of mild steel in 1.0 M H_2SO_4 solution in the absence and presence of different concentrations of the complex C4 at 25 °C

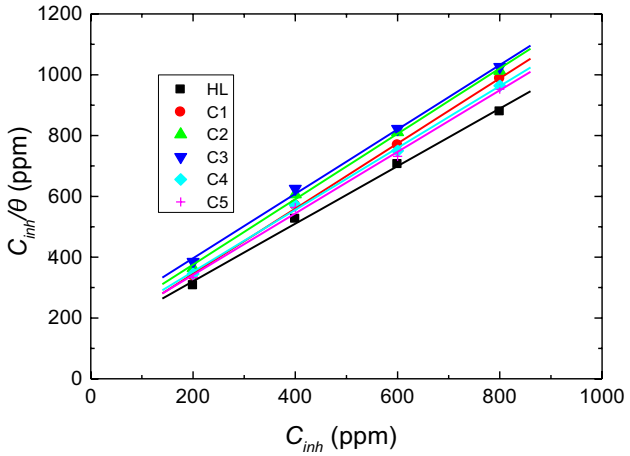

Fig. 10 Langmuir adsorption isotherms for the synthesized ligand (HL) and its complexes (**C1** to **C5**) adsorbed on mild steel surface in 1.0 M H_2SO_4 solution at 25 °C

afford knowledge about the adsorption mode of the inhibitor molecules. The values of fractional surface coverage (C_{inh}/θ) for the investigated compounds in 1.0 M H_2SO_4 solution, obtained from weight-loss measurements, were plotted against inhibitors concentrations (C_{inh}) and are illustrated in Fig. 10. These plots were found to be straight lines with approximately unit slopes indicating that the adsorption of the tested compounds on mild steel surface in 1.0 M H_2SO_4 solution agree with the Langmuir adsorption isotherm which is given by following equation [58]:

$$\frac{C_{inh}}{\theta} = \frac{1}{K_{ads}} + C_{inh} \quad (3)$$

where K_{ads} is the equilibrium constant of adsorption.

4 Conclusion

Five Novel divalent and trivalent metal chelates of the ligand named (E)-1-((4,6-dimethylpyrimidin-2-ylimino)methyl) naphthalen-2-ol were isolated by the reaction of the ligand with different metal chlorides. The isolated complexes have been proved by the analytical tools $[L_2Cu]$, $[L_2Co(H_2O)_2]H_2O$, $[L_2Ni(H_2O)_2]2H_2O$, $[LFe(H_2O)_2Cl_2]0.5H_2O$ and $[LCd(H_2O)_3Cl]$, where L is the deprotonated ligand. The binding mode of the ligand to the metal and geometrical structures of the metal chelates has been successfully deduced using the IR spectra confirming monobasic bidentate behavior of the ligand connecting the metal ion centers via deprotonated phenolic OH and imine nitrogen. In the case of Cu(II) complex, the pyrimidine nitrogen took part in coordination to the Cu center. UV–Vis spectra and magnetic moment confirmed the octahedral geometry around the metal center. The X-ray single crystal structure of the ligand has been also discussed. Values of the molar conductance that all metal complexes are non-electrolytic type of complexes. The antimicrobial activities of the synthesized metal chelates were evaluated against different bacterial and fungal strains. The obtained data displayed that the metal chelates had high activity against the tested bacterial and fungal strains and complex **C5** showed increased activity over all the other metal complexes and also the slandered drugs. The synthesized ligand and its complexes were employed as efficient inhibitors for the corrosion of mild steel in 1.0 M H_2SO4 solution. Adsorption of the tested compounds on mild steel follows the Langmuir adsorption isotherms. The extent of inhibition efficiencies of the compounds followed the order: **HL > C5 > C4 > C1 > C2 > C3**. The results obtained from the applied techniques are compatible with each other.

5 Supplementary Materials

The crystallographic supporting results of HL are found on CCDC 1888982. These data can be obtained reaching the link http://www.ccdc.cam.ac.uk/conts/retrieving.html or directly from the Cambridge Crystallographic Data Center.

References

1. P.S. Theivendren, C.R. James, P.V. Dniandev, S.K. Valzita, A mini review of pyrimidine and fused pyrimidine marketed drugs. Res. Pharm. **2**, 1–9 (2012)

2. V. Sharma, N. Chitranshi, A.K. Agarwa, Significance and biological importance of pyrimidine in the microbial world. Inter. J. Med. Chem. **2014**, 1–31 (2014)
3. M. Sonmez, M. Celebi, I. Berber, Synthesis, spectroscopic and biological studies on the new symmetric Schiff base derived from 2,6-diformyl-4-methylphenol with N-aminopyrimidine. Eur. J. Med. Chem. **45**, 1935–1940 (2010)
4. J.I. Pyo, E.J. Hwang, C.S. Cheong, S.H. Lee, S.W. Lee, I.T. Kim, S.H. Lee, Synthesis and photoluminescent properties of novel furopyrimidine derivatives. Synth. Met. **155**, 461–463 (2005)
5. M. Sonmez, M.E. Hacıyusufoglu, A. Levent, H. Zengin, G. Zengin, Synthesis of pyrimidine Schiff base transition metal complexes: characterization, spectral and electrochemical analyses, and photoluminescence properties. Res. Chem. Intermed. **44**, 5531–5546 (2018)
6. A. Elsherbiny, H. El-Ghamry, Synthesis, characterization, and catalytic activity of new Cu(II) complexes of Schiff base: effective catalysts for decolorization of acid red 37 dye solution. Int J. Chewm. Kinet. **47**, 162–173 (2015)
7. K.C. Gupta, A.K. Sutar, Catalytic activities of Schiff base transition metal complexes. Coord. Chem. Rev. **252**, 1420–1450 (2008)
8. A. Prakash, D. Adhikari, Application of Schiff bases and their metal complexes—a review. Int. J. Chem. Technol. Res. **3**, 1891–1896 (2011)
9. S. Kumar, D.N. Dhar, P.N. Saxena, Applications of metal complexes of Schiff bases-a review. J. Sci. Ind. Res. **68**, 181–187 (2009)
10. S. Arulmurugan, H.P. Kavitha, B.R. Venkatraman, Biological activities of Schiff base and its complexes: a review. Rasayan J. Chem. **3**, 385–410 (2010)
11. S. Rostamnia, A. Morsali, Basic isoreticular nanoporous metal–organic framework for Biginelli and Hantzsch coupling: IRMOF-3 as a green and recoverable heterogeneous catalyst in solvent-free conditions. RSC Adv. **4**, 10514–10518 (2014)
12. M. Gaber, N.A. El-Wakiel, H.A. El-Ghamry, S.K. Fathalla, Synthesis, spectroscopic characterization, DNA interaction and biological activities of Mn(II), Co(II), Ni(II) and Cu(II) complexes with [(1H-1,2,4-triazole-3-ylimino)methyl]naphthalene-2-ol. J. Mol. Str. **1076**, 251–261 (2014)
13. M. Gaber, H.A. El-Ghamry, F. Atlam, S.K. Fathalla, Synthesis, spectral and theoretical studies of Ni(II), Pd(II) and Pt(II) complexes of 5-mercapto-1,2,4-triazole-3-imine-2′-hydroxynaphyhaline. Spectrochim. Acta A **137**, 919–929 (2015)
14. M. Gaber, H.A. El-Ghamry, S.K. Fathalla, Ni(II), Pd(II) and Pt(II) complexes of (1H-1,2,4-triazole-3-ylimino)methyl]naphthalene-2-ol. Structural, spectroscopic, biological, cytotoxicity, antioxidant and DNA binding. Spectrochim. Acta A **139**, 396–404 (2015)
15. R. Drozdzak, B. Allaert, N. Ledoux, I. Dragutan, V. Dragutan, F. Verpoort, Coord. Chem. Rev. **249**, 3055–3074 (2005)
16. S. Rostamnia, H. Alamgholiloo, X. Liu, Pd-grafted open metal site copper-benzene-1,4-dicarboxylate metal organic frameworks (Cu-BDC MOF's) as promising interfacial catalysts for sustainable suzuki coupling. J. Colloid Interf. Sci **469**, 310–317 (2016)
17. H. Alamgholiloo, S. Rostamnia, A. Hassankhani, J. Khalafy, M.M. Baradarani, G. Mahmoudi, X. Liu, Stepwise post-modification immobilization of palladium Schiff-base complex on to the OMS-Cu (BDC) metal–organic framework for Mizoroki-Heck cross-coupling reaction. App. Organomet. Chem. **32**, e4539 (2018)
18. S. Samadhiya, A. Halve, Synthetic utility of Schiff bases as potential herbicidal agents. Orient. J. Chem. **17**, 87–94 (2001)
19. K.Y. El-Baradie, N.A. El-Wakiel, H.A. El-Ghamry, Synthesis, characterization and corrosion inhibition in acid medium of L-histidine Schiff base complexes. Appl. Organometal. Chem. **29**, 117–125 (2015)
20. M. Behpour, S.M. Ghoreishi, N. Mohammadi, M.S. Niasari, Damage analysis and cracking model of reinforced concrete structures with rebar corrosion. Corros. Sci. **53**, 3380–3397 (2011)
21. C. Kustu, K.C. Emregul, O. Atakol, Schiff bases of increasing complexity as mild steel corrosion inhibitors in 2 M HCl. Corros. Sci. **49**, 2800–2814 (2007)
22. M. Behpour, S.M. Ghoreishi, N. Soltani, M.S. Niasari, The inhibitive effect of some bis-N, S-bidentate Schiff bases on corrosion behaviour of 304 stainless steel in hydrochloric acid solution. Corros. Sci. **51**, 1073–1082 (2009)
23. A. Fawzy, I.A. Zaafarany, H.M. Ali, M. Abdallah, New synthesized amino acids-based surfactants as efficient inhibitors for corrosion of mild Steel in hydrochloric acid medium: kinetics and thermodynamic approach. Int. J. Electrochem. Sci. **13**, 4575–4600 (2018)
24. A. Fawzy, M. Abdallah, I.A. Zaafarany, S.A. Ahmed, I.I. Althagafi, Thermodynamic, kinetic and mechanistic approach to the corrosion inhibition of carbon steel by new synthesized amino acids-based surfactants as green inhibitors in neutral and alkaline aqueous media. J. Mol. Liq. **265**, 276–291 (2018)
25. M. Abdallah, O.A. Hazazi, A. Fawzy, S. El-Shafei, A.S. Fouda, Influence of N-thiazolyl-2-cyanoacetamide derivatives on the corrosion of aluminum in 0.01 M sodium hydroxide. Prot. Met. Phys. Chem. Surf. **50**, 659–666 (2014)
26. M.I. Awad, A.F. Saad, M.R. Shaaban, B.A.A.L. Jahdaly, O.A. Hazazi, New insight into the mechanism of the inhibition of corrosion of mild steel by some amino acids. Int. J. Electrochem. Sci. **12**, 1657–1669 (2017)
27. O.A. Hazazi, A. Fawzy, M.R. Shaaban, M.I. Awad, Enhanced 4-amino-5-methyl-4H-1,2,4-triazole-3-thiol inhibition of corrosion of mild steel in 0.5 M H_2SO_4 by Cu(II). Int. J. Electrochem. Sci. **9**, 1378–1389 (2014)
28. M. Abdallah, A.S. Fouda, I. Zaafarany, A. Fawzy, Y. Abdallah, Corrosion inhibition of iron in sulphuric acid solution by antibacterial cephalosporin. J. Am. Sci. **9**, 209–215 (2013)
29. F. Bentiss, M. Lagrenée, M. Traisnel, J.C. Hornez, The corrosion inhibition of mild steel in acidic media by a new triazole derivative. Corros. Sci. **41**, 789–803 (1999)
30. O.A. Hazazi, A. Fawzy, M.I. Awad, Synergistic effect of halides on the corrosion inhibition of mild steel in H_2SO_4 by a triazole derivative: kinetics and thermodynamic studies. Int. J. Electrochem. Sci. **9**, 4086–4103 (2014)
31. F. Bentiss, M. Lagrenée, M. Traisnel, 2,5-bis(n-pyridyl)-1 3,4-oxadiazoles as corrosion inhibitors for mild steel in acidic media. J. Corros. **56**, 733–742 (2000)
32. M. Abdallah, M.M. Salem, A. Fawzy, E.M. Mabrouk, Electrochemical behavior of nickel alloys and stainless steel in HNO_3 using cyclic voltammetry technique. J. Mater. Env. Sci. **8**, 1320–1327 (2017)
33. R.F. Godec, M.G. Pavlovic, Synergistic effect between non-ionic surfactant and halide ions in the forms of inorganic or organic salts for the corrosion inhibition of stainless-steel X_4Cr_{13} in sulphuric acid. Corros. Sci. **58**, 192–201 (2012)
34. M. Abdallah, I. Zaafarany, A. Fawzy, M.A. Radwan, E. Abdfattah, Inhibition of aluminum corrosion in hydrochloric acid by cellulose and chitosan. J. Am. Sci. **9**, 580–586 (2013)
35. O.A. Hazazi, A. Fawzy, M.I. Awad, Sulfachloropyridazine as an eco-friendly inhibitor for corrosion of mild steel in H_2SO_4 solution. Chem. Sci. Rev. Lett. **4**, 67–79 (2015)
36. A.A. Osowole, R. Kempe, R. Schobert, K. Effenberger, Synthesis, spectroscopic, thermal, and in vitro anticancer properties of some M(II) complexes of 3-(-1-(4,6-dimethyl-2-pyrimidinylimino) methyl-2-naphthol. Synth. React. Inorg. Met. Org. Nano-Met. Chem. **41**, 825–833 (2011)
37. N.H. Yarkandi, H.A. El-Ghamry, M. Gaber, Synthesis, spectroscopic and DNA binding ability of Co^{II}, Ni^{II}, Cu^{II} and Zn^{II}

complexes of Schiff base ligand (E)-1-(((1H-benzo[d]imidazol-2-yl) methylimino)methyl)naphthalen-2-ol. X-ray crystal structure determination of cobalt(II) complex. Mater. Sci. Eng. C **75**, 1059–1067 (2017)
38. A. Bauer, W. Kirby, C. Sherris, M. Turck, Antibiotic susceptibility testing by a standardized single disk method. Am. J. Clin. Pathol. **45**, 493–496 (1966)
39. M. Pfaller, L. Burmeister, M.A. Bartlett, M.G. Rinaldi, J. Clin. Microbiol. **26**, 1437–1441 (1988)
40. F.H. Allen, O. Kennard, D.G. Watson, L. Brammer, A.G. Open, R. Taylor, Tables of bond lengths determined by X-ray and neutron diffraction. Part 1. Bond lengths in organic compounds. J. Chem. Soc. Perkin Trans. **12**, S1–19 (1987)
41. R. Pradhan, M. Banik, D.B. Cordes, A.M.Z. Slawin, N.C. Saha, Synthesis, characterization, X-ray crystallography and DNA binding activities of Co(III) and Cu(II) complexes with a pyrimidine-based Schiff. Inorg. Chim. Acta **442**, 70–80 (2016)
42. L.B. Tang, G.N. Mu, G.H. Liu, The effect of neutral red on the corrosion inhibition of cold rolled steel in 1.0 M hydrochloric acid. Corros. Sci. **45**, 2251–2262 (2003)
43. A. Majumder, G.M. Rosair, A. Mallick, N. Chattopadhyay, S. Mitra, Synthesis, structures and fluorescence of nickel, zinc and cadmium complexes with the *N*, *N*, *O*-tridentate Schiff base *N*-2-pyridylmethylidene-2-hydroxy-phenylamine. Polyhedron **25**, 1753–1762 (2006)
44. K. Singh, M.S. Barwa, P. Tyagi, Synthesis, characterization and biological studies of Co(II), Ni(II), Cu(II) and Zn(II) complexes with bidentate Schiff bases derived by heterocyclic ketone. Eur. J. Med. Chem. **41**, 147–153 (2006)
45. H.A. El-Ghamry, S.K. Fathalla, M. Gaber, Synthesis, structural characterization and molecular modelling of bidentateazo dye metal complexes: DNA interaction to antimicrobial and anticancer activities. Appl. Organometal. Chem. **32**, e4136 (2017)
46. R. Holman, M.P. Hendrich, L. Que Jr., EPR studies of a dinickel complex in its (II, II) and (II, III) oxidation states. Inorg. Chem. **31**, 937–939 (1992)
47. R. Paulpandiyan, N. Raman, DNA binding propensity and nuclease efficacy of biosensitive Schiff base complexes containing pyrazolone moiety: synthesis and characterization. J. Mol. Str. **1125**, 374–382 (2016)
48. H. Liu, H. Wang, F. Gao, D. Niu, Z. Lu, Self-assembly of copper(II) complexes with substituted aroylhydrazones and monodentate N-heterocycles: synthesis, structure and properties. J. Coord. Chem. **60**, 2671–2678 (2007)
49. A.M. Gouda, H.A. El-Ghamry, T.M. Bawazeer, T.A. Farghaly, A.N. Abdalla, A. Aslam, Antitumor activity of pyrrolizines and their Cu(II) complexes: design, synthesis and cytotoxic screening with potential apoptosis-inducing activity. Eur. J. Med. Chem. **145**, 350–359 (2018)
50. A.B.P. Lever, *Inorganic Electronic Spectroscopy*, 2nd edn. (Elsevier, Amsterdam, 1984)
51. K. El-Baradie, R. El-Sharkawy, H. El-Ghamry, K. Sakai, Synthesis and characterization of Cu(II), Co(II) and Ni(II) complexes of a number of sulfadrugazodyes and their application for wastewater treatment. Spectrochim. Acta A **121**, 180–187 (2014)
52. E.V. Zahınos, M.A.M. Rogado, F.L. Giles, F.J.B. Garcıa, Coordination behaviour of Schiff base 2-acetyl-2-thiazoline hydrazone (ATH) towards cobalt(II), nickel(II) and copper(II). Polyhedron **27**, 879–886 (2008)
53. Y.K. Abdel-Monem, S.A. Abouel-Enein, S.M. El-Seady, Synthesis, characterization and molecular modeling of some transition metal complexes of Schiff base derived from 5-aminouracil and 2-benzoyl pyridine. J. Mol. Struct. **1152**, 115–127 (2018)
54. D.N. Kumar, B.S. Garg, Synthesis and spectroscopic studies of complexes of zinc(II) with N_2O_2 donor groups. Spectrochim. Acta A **64**, 141–147 (2006)
55. R.S. Joseyphus, M.S. Nair, Antibacterial and antifungal studies on some Schiff base complexes of zinc(II). Microbiology **36**, 93–98 (2008)
56. G.N. Mu, X.H. Li, Q. Qu, J. Zhou, Molybdate and tungstate as corrosion inhibitors for cold rolling steel in hydrochloric acid solution. Corros. Sci. **48**, 445–459 (2006)
57. C. Hsu, F. Mansfeld, Technical note concerning the conversion of the constant phase element parameter Y_0 into a capacitance. Corrosion **57**, 747–748 (2001)
58. M. Christov, A. Popova, Adsorption characteristics of corrosion inhibitors from corrosion rate measurements. Corros. Sci. **46**, 1613–1620 (2004)